

Iterative fluctuation ghost imaging

HUAN ZHAO¹, XIAO-QIAN WANG^{1,**}, CHAO GAO¹, ZHUO YU^{1,2}, HONG WANG¹, YU WANG¹, LI-DAN GOU¹, AND ZHI-HAI YAO^{1,*}

¹Department of Physics, Changchun University of Science and Technology, Changchun 130022, China

²School of Physics and Electronics, Baicheng Normal University, Baicheng 137000, China

*Corresponding author: yaozhi@cust.edu.cn

**Corresponding author: xqwang21@163.com

Compiled April 25, 2023

We present a new technique, iterative fluctuation ghost imaging (IFGI) which dramatically enhances the resolution of ghost imaging (GI). It is shown that, by the fluctuation characteristics of the second-order correlation function, the imaging information with the narrower point spread function (PSF) than the original information can be got. The effects arising from the PSF and the iteration times also be discussed.

© 2023 Optical Society of America

<http://dx.doi.org/10.1364/ao.XX.XXXXXX>

Ghost imaging (GI) is an imaging technique based on second-order intensity correlation[1–11]. It has various novel advantages for practical applications compared with traditional imaging, such as resistant of atmosphere turbulence[12, 13] and lensless imaging [3, 4]. GI has been applied in various fields including optical lithography[14], remote imaging[15], microscopy imaging[16], x-ray imaging[17] and imaging for an occluded object[7]. In these applications, the spatial resolution of image is an important factor[18]. How to improve the resolution of GI is a key factor in the development of GI[18–21].

In traditional imaging systems, the resolution is given by Rayleigh criterion[5]. It comes from the point spread function (PSF) of the imaging system. Many schemes have been proposed to enhance resolution via reducing the impact of PSF[22, 23]. In GI systems, the spatial resolution is also limited by the Rayleigh diffraction bound just as in traditional imaging, when the pixel size of the detector is much smaller than the average size of the speckles[18, 19]. In general, it is taken to be the full-width at half-maximum (FWHM) of the PSF, and is approximately equal to the average size of the speckles[5, 18, 24]. Some schemes to improve the spatial resolution of GI have also been proposed. Han's group reported a two-arm microscope scheme by employing second-order intensity correlation imaging to narrow PSF[25]. Compressed sensing GI (CSGI) reduces the effect of PSF on the imaging quality using sparsity constraints to improve the spatial resolution of GI[21, 26–28]. Shih's group report a super-resolution method which using the spatial-frequency filtered intensity fluctuation correlation to reduce the FWHM of PSF[29]. The narrowing of PSF by higher-order correlation

of non-Rayleigh speckle fields has been reported[30]. A sub-Rayleigh resolution ghost imaging experiment is performed by spatial low-pass filtering of the instantaneous intensity to narrow PSF[18]. Li's group used localizing and thresholding to reduce the effect of PSF in the GI system[31]. Other schemes to enhance the resolution of GI by reducing the effect of the PSF have also been suggested, such as preconditioned deconvolution methods[32], deep neural network constraints[33], speeded up robust features new sum of modified Laplacian (SURF-NSML)[34], high-resolution ghost imaging through complex scattering media via a temporal correction[35] and second-order cumulants ghost imaging (SCGI)[36].

In this work, we propose a scheme based on traditional thermal GI. It can narrow the PSF of the GI via the fluctuation characteristics of the second-order correlation function. And further extraction of deep-seated fluctuation information via iterations, the PSF can further become narrow. Based on this effect, the scheme can significantly enhance the resolution of GI system until the resolution approaches the pixel size of the detector. We called the scheme iterative fluctuation ghost imaging (IFGI). Compare to SCGI, there is no cross-information in IFGI. Thus, IFGI has higher resolution limits than SCGI.

The principle of the experiment is shown in Fig. 1. It is similar to the traditional GI system[18], but each beam contains a spatially resolving charge-coupled device (CCD) detector CCD_i ($i = 1, 2$) in the system. x , α and β are the transverse coordinates on the source plane, object plane and imaging plane, respectively. The distance from the source to the object plane and image plane are s_o and s_i , respectively.

In this system, we consider that the source is monochromatic light with a wavelength λ . The light field PSF from source to object and from source to CCD_2 are written as

$$h_t(x, \alpha) = \frac{e^{-iks_o}}{i\lambda s_o} \exp\left(\frac{-i\pi}{\lambda s_o}(x - \alpha)^2\right), \quad (1)$$

$$h_r(x, \beta) = \frac{e^{-iks_i}}{i\lambda s_i} \exp\left(\frac{-i\pi}{\lambda s_i}(x - \beta)^2\right), \quad (2)$$

where $k = \frac{2\pi}{\lambda}$. The light intensity distribution on the object and CCD_2 plane are represented as $I(\alpha)$ and $I(\beta)$, respectively. The transmission function of the object is represented as $t(\alpha)$. Then, we can get that the correlation between the intensity fluctuations

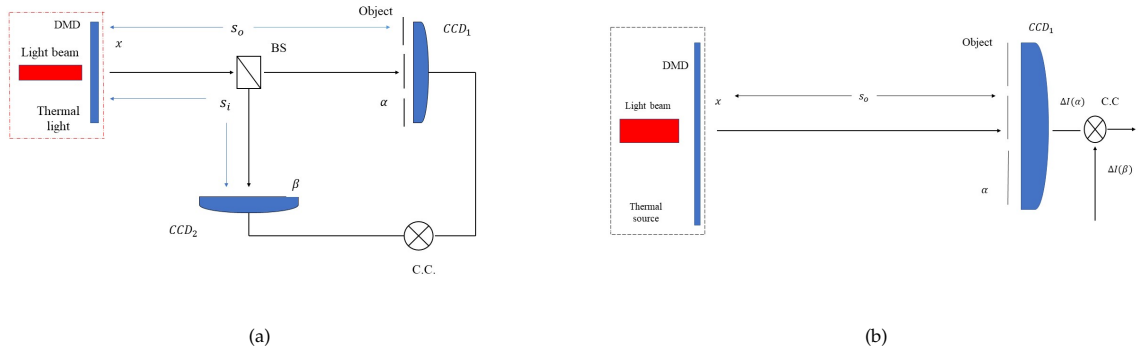


Fig. 1. (a) Schematic diagram of the experimental setup; (b) Schematic of simplified single-arm setup, which is equivalent to (a);

at two detectors is

$$\begin{aligned} \Delta G^{(2)}(\alpha, \beta) &= \langle [I(\alpha)|t(\alpha)|^2 - \langle I(\alpha)|t(\alpha)|^2][I(\beta) - \langle I(\beta) \rangle] \rangle \\ &= \langle \Delta I(\alpha)|t(\alpha)|^2 \Delta I(\beta) \rangle \\ &= \left| \int G^{(1)}(x, x') t(\alpha) h_t(x, \alpha) h_r^*(x', \beta) dx dx' \right|^2, \end{aligned} \quad (3)$$

where $\langle \dots \rangle$ represents the ensemble average. We consider a situation where light comes as a point-like source which is randomly and uniformly distributed on the source plane, then

$$G^{(1)}(x, x') = I_0 \delta(x - x'), \quad (4)$$

where I_0 is the intensity of the source and $\delta(x)$ is the Dirac delta function. We further consider that $s_o = s_i = z$. Then, substituting Eqs. (1-2) and Eq. (4) into Eq. (3), after some calculations, we have

$$\begin{aligned} \Delta G^{(2)}(\alpha, \beta) &= \langle \Delta I(\alpha)|t(\alpha)|^2 \Delta I(\beta) \rangle \\ &= I_0^2 \times |t(\alpha)|^2 \text{sinc}^2\left(\frac{2\pi R}{\lambda z}(\alpha - \beta)\right). \end{aligned} \quad (5)$$

We integral the all $\Delta I(\alpha)|t(\alpha)|^2$ by CCD_1 , the corresponding ghost image is given by

$$\Delta G^{(2)}(\beta) = \langle \Delta I(\beta) \Delta B_t \rangle = I_0^2 \int |t(\alpha)|^2 \text{sinc}^2\left(\frac{2\pi R}{\lambda z}(\alpha - \beta)\right) d\alpha, \quad (6)$$

where $\Delta B_t = \int \Delta I(\alpha)|t(\alpha)|^2 d\alpha$, i.e., the intensity fluctuation at the bucket detector of GI system.

If we consider that the power of the source cannot be kept stable, the $\Delta G^{(2)}(\alpha, \beta)$ in Eq. (5) and $\Delta G^{(2)}(\beta)$ in Eq. (6) should be substituted with $\Delta G^{(2)}(I_0, \alpha, \beta)$ and $\Delta G^{(2)}(I_0, \beta)$, respectively. Fluctuations of I_0 lead to fluctuations of $\Delta G^{(2)}(I_0, \alpha, \beta)$ and $\Delta G^{(2)}(I_0, \beta)$ [36]. We use cumulants to describe their fluctuations information. For $\Delta G^{(2)}(I_0, \alpha, \beta)$, the cumulant-generating function $K(s, \alpha, \beta)$ is defined as

$$\begin{aligned} K(s, \alpha, \beta) &= \ln(\langle \exp(s \Delta G^{(2)}(I_0, \alpha, \beta)) \rangle) = \sum_{n=1}^{\infty} \kappa_n(\alpha, \beta) \frac{s^n}{n!} \\ &= \mu(\alpha, \beta) \times s + \sigma^2(\alpha, \beta) \times \frac{s^2}{2} + \dots, \end{aligned} \quad (7)$$

where $\kappa_n(\alpha, \beta)$ is the n th-order cumulants of $\Delta G^{(2)}(I_0, \alpha, \beta)$, $\mu(\alpha, \beta) = \langle \Delta G^{(2)}(I_0, \alpha, \beta) \rangle$, and $\sigma^2(\alpha, \beta) = \langle [\Delta G^{(2)}(I_0, \alpha, \beta) - \mu(\alpha, \beta)]^2 \rangle$. The n th-order cumulants is given by

$$\kappa_n(\alpha, \beta) = \frac{d^{(n)} K(s, \alpha, \beta)}{ds^{(n)}} \Big|_{s=0}. \quad (8)$$

From Eqs. (7-8), we can get the second-order cumulant of $\Delta G^{(2)}(I_0, \alpha, \beta)$ as

$$\begin{aligned} \kappa_2(\alpha, \beta) &= \langle [\Delta G^{(2)}(I_0, \alpha, \beta) - \langle \Delta G^{(2)}(I_0, \alpha, \beta) \rangle]^2 \rangle \\ &= \langle (I_0 - \langle I_0 \rangle)^2 \rangle \times |t(\alpha)|^4 \text{sinc}^4\left(\frac{2\pi R}{\lambda z}(\alpha - \beta)\right). \end{aligned} \quad (9)$$

From Eq. (9), we can get that $\kappa_2(\alpha, \beta)$ is the fluctuation information of $\Delta G^{(2)}(I_0, \alpha, \beta)$. Compare Eq. (5) with Eq. (9), we also can get that it has narrower PSF than that of $\Delta G^{(2)}(I_0, \alpha, \beta)$. Then, we integral the all $\kappa_2(\alpha, \beta)$ by the CCD_1 , and get the new imaging information as

$$\begin{aligned} \kappa_2^{(1)}(\beta) &= \int \kappa_2(\alpha, \beta) d\alpha \\ &= \langle (I_0 - \langle I_0 \rangle)^2 \rangle \times \int |t(\alpha)|^4 \text{sinc}^4\left(\frac{2\pi R}{\lambda z}(\alpha - \beta)\right) d\alpha. \end{aligned} \quad (10)$$

Compare to traditional GI in Eq. (6), Eq. (10) use $\kappa_2^{(1)}(\beta)$ instead of $\Delta G^{(2)}(I_0, \beta)$ to get the information of the object, and has the narrower PSF. So, it has the better resolution than traditional GI. From Eq. (9), we also can get that the fluctuations of I_0 lead to fluctuations of $\kappa_2(\alpha, \beta)$. Similarly, we can further enhance the resolution of GI by the integral fluctuation information of $\kappa_2(\alpha, \beta)$. It is written as

$$\begin{aligned} \kappa_2^{(2)}(\beta) &= \int \frac{d^{(2)} \ln(\langle \exp(s \kappa_2(\alpha, \beta)) \rangle)}{ds^{(2)}} \Big|_{s=0} d\alpha \\ &\propto \int |t(\alpha)|^8 \text{sinc}^8\left(\frac{2\pi R}{\lambda z}(\alpha - \beta)\right) d\alpha. \end{aligned} \quad (11)$$

If we use $\kappa_2^{(0)}(\alpha, \beta)$, $\kappa_2^{(1)}(\alpha, \beta)$ and $\kappa_2^{(2)}(\alpha, \beta)$ to represent $\Delta G^{(2)}(I_0, \alpha, \beta)$, $\Delta G^{(2)}(I_0, \beta)$ and $\kappa_2(\alpha, \beta)$, respectively, according to Eq. (6) and Eqs. (10-11), we can get

$$\begin{aligned} \kappa_2^{(n)}(\beta) &= \int \frac{d^{(2)} \ln(\langle \exp(s \kappa_2^{(n-1)}(\alpha, \beta)) \rangle)}{ds^{(2)}} \Big|_{s=0} + \delta(n) [\kappa_2^{(0)}(\alpha, \beta) \\ &\quad - \frac{d^{(2)} \ln(\langle \exp(s \kappa_2^{(n-1)}(\alpha, \beta)) \rangle)}{ds^{(2)}} \Big|_{s=0}] d\alpha = \int \kappa_2^{(n)}(\alpha, \beta) d\alpha, \end{aligned} \quad (12)$$

where n is iteration times. Each iteration means that we go one step further to extract the fluctuation information. From Eq. (12), we can get that $\kappa_2^{(n)}(\beta)$ is the information consisting of all $\kappa_2^{(n)}(\alpha, \beta)$. $\kappa_2^{(n)}(\alpha, \beta)$ is the fluctuation information of $\kappa_2^{(n-1)}(\alpha, \beta)$ when $n \geq 1$. It is equivalent to $\Delta G^{(2)}(I_0, \alpha, \beta)$

when $n = 0$. After calculation Eq. (12), we can get that the PSF of $\kappa_2^{(n)}(\beta)$ will become narrower as n grows. In order to address a concrete example, we set $\lambda = 628\text{nm}$, $z = 0.25\text{m}$ and $R = 1\text{mm}$. For a pinhole-like object at $\alpha = 0$, the imaging results by Eq. (12) (here, we set $n=1,2,3$) are shown in Fig. 2. The physical signifi-

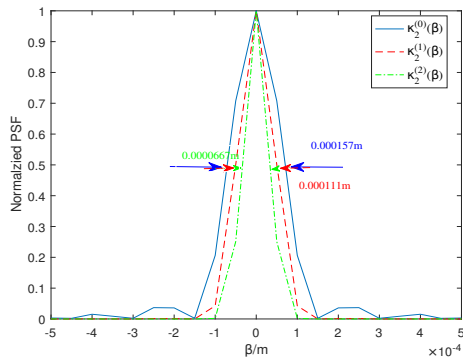


Fig. 2. PSF of a pinhole object at $\alpha = 0$ and $\lambda = 628\text{nm}$, $z = 0.25\text{m}$ and $R = 1\text{mm}$ by $\kappa_2^{(0)}(\beta)$ (blue solid curve), $\kappa_2^{(1)}(\beta)$ (red dash curve) and $\kappa_2^{(2)}(\beta)$ (green dotted curve).

cance is that when the $\kappa_2^{(n-1)}(\alpha, \beta)$ (here $n \geq 1$) has the image information about α points on the object plane. Its fluctuation information not only has the information about α points, but also has the narrower PSF than that of the original information. So, $\kappa_2^{(n)}(\beta)$ has the better resolution than that of $\kappa_2^{(n-1)}(\beta)$.

Due to $\kappa_2^{(n)}(\alpha, \beta)$ is the fluctuation information of $\kappa_2^{(n-1)}(\alpha, \beta)$, the signal strength of $\kappa_2^{(n)}(\alpha, \beta)$ is weaker than that of $\kappa_2^{(n-1)}(\alpha, \beta)$. So, although increasing the n of the $\kappa_2^{(n)}(\beta)$ leads to the decrease of the FWHM of the PSF, it also results in the decrease of the signal strength. We can set n according to imaging requirements. The scheme which used $\kappa_2^{(n)}(\beta)$ to get the image of the object, is called iterative fluctuation ghost imaging (IFGI). It is equivalent a traditional GI when $n = 0$.

In our previous work[36], we have presented a scheme for GI referred to as SCGI. It is shown that $\kappa_2(\beta)$ is the fluctuation information of $\Delta G^{(2)}(I_0, \beta)$, and has better resolution than that of $\Delta G^{(2)}(I_0, \beta)$. In [36], we can get that $\kappa_2(\beta)$ not only has $\kappa_2^{(1)}(\beta)$, but also has a cross-information $L(\beta)$ which reduce the resolution. This is because that in the framework of SCGI, it can get the $\Delta G^{(2)}(I_0, \beta)$ that is the correlation between the intensity fluctuations at β point and bucket detector, but it cannot get the $\Delta G^{(2)}(I_0, \alpha, \beta)$ that is the correlation between the intensity fluctuations at α point and β point. The fluctuation information of $\Delta G^{(2)}(I_0, \beta)$ not only include the fluctuation information of $\Delta G^{(2)}(I_0, \alpha, \beta)$ for different α points, but also include the cross-information between them, which cannot distinguish. However, we used CCD_1 instead of a bucket detector in IFGI. If the distance between the object and the CCD_1 is smaller than their longitudinal coherence length, it can get the information of the $\Delta G^{(2)}(I_0, \alpha, \beta)$. So $L(\beta)$ is disappear in IFGI. IFGI has the better resolution limit than SCGI.

To verify our theoretical results, experiment results are carried out. We use the simple single-arm setup shown in Fig. 1(b) (it is equivalent to Fig. 1(a)[18]). The light source is a projector (XE11F), and there is a digital mirror device (DMD) in the source.

An double slit with width $a = 0.223\text{mm}$, slits center distance $b = 0.445\text{mm}$, and slit height $g = 1.114\text{mm}$ as the object. It is shown in Fig. 3. The distance between the source plane and the object is 25cm . A camera (MV-VEM033SM) is taken as CCD_1 . The experimental process is as follows: a series of transverse patterns are generated by computer. Each pattern is projected by a projector and illuminates the object, and the transmitted light is collected by a CCD_1 . After 20000 measurements, we get 20000 group $I(\alpha)$. Then, we move the object. Above patterns are re-projected and directly received by CCD_1 , respectively. We get 20000 group $I(\beta)$. In this experiment, we use CCD_1 , traditional GI and IFGI to get the image of the object, respectively. The results are shown in Fig. 4.

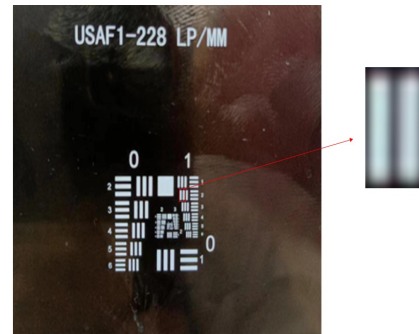


Fig. 3. The test object for this experiment.

From Figs. 4(a-b), we can find that the resolution of the image by CCD_1 is better than that by traditional GI. This is because that the distance between the source and the object is far greater than the distance between the object and the CCD_1 in this system. From Figs. 4(b-d), we can get that the double slit cannot be separated by traditional GI (see Fig. 4(b)). However, it can be separated by IFGI and increasing the n of $\kappa_2^{(n)}(\beta)$ leads to the enhancement of the resolution of IFGI (see Figs. 4(c-d)). According to our previous analysis, the resolution of GI system is limited by the PSF, and $\kappa_2^{(n)}(\alpha, \beta)$ has the narrower PSF than $\kappa_2^{(n-1)}(\alpha, \beta)$. So, $\kappa_2^{(n)}(\beta)$ has the better resolution than $\kappa_2^{(n-1)}(\beta)$. Compare Fig. 4(a) with Fig. 4(d), we can get that the resolution of IFGI is better than that by CCD_1 . IFGI can enhance the resolution of GI via extract the fluctuation information as n grows, until its resolution is close the pixel size of the detector. The experimental results agree with our theoretical analysis.

Compare Fig. 4(b) with Fig. 4(c), we can also get that the signal strength of traditional GI is better than that of IFGI. This is because that $\kappa_2^{(1)}(\alpha, \beta)$ is the fluctuation information of $\Delta G^{(2)}(I_0, \alpha, \beta)$. Compare Fig. 4(c) with Fig. 4(d), we also get that the signal strength of $\kappa_2^{(2)}(\beta)$ is weaker than $\kappa_2^{(1)}(\beta)$. This is because that $\kappa_2^{(n)}(\alpha, \beta)$ is the fluctuation information of $\kappa_2^{(n-1)}(\alpha, \beta)$ when $n \geq 1$. Above experimental results proved that the resolution of IFGI become better and the signal strength become weaker as n grows. In any case, we can have a tradeoff according to the image requirements.

In conclusion, we have presented a technique called IFGI that enhances dramatically the resolution of the GI via the fluctuation characteristics of the second-order correlation function. It is found that the resolution is strongly dependent on the iteration times n when the pixel size of the detector is much smaller than

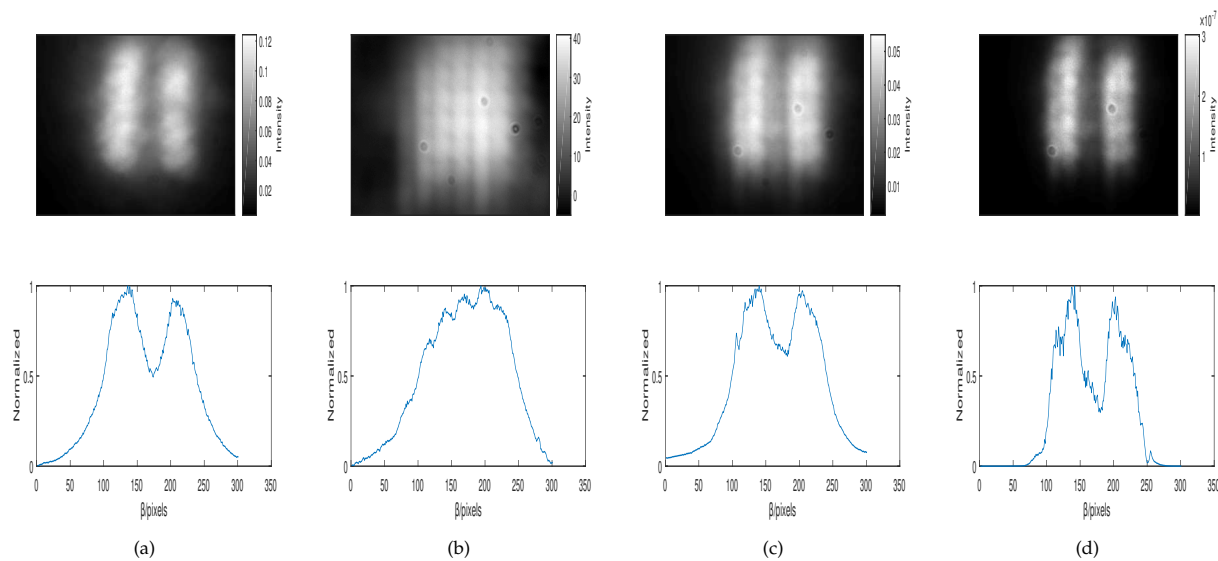


Fig. 4. The reconstructed images of the object by CCD_1 , traditional GI and IFGI; (a) CCD_1 ; (b) traditional GI; (c) IFGI($\kappa_2^{(1)}(\beta)$); (d) IFGI($\kappa_2^{(2)}(\beta)$);

the average size of the speckles. Although a trade-off between resolution and signal strength has to be considered, we select n according to the image requirements. It offers a general and alternative approach applicable to all fields of imaging where higher resolution is needed.

ACKNOWLEDGEMENT

This work is supported by the Science & Technology Development Project of Jilin Province (No.YDZJ202101ZYTS030).

DISCLOSURES

Disclosures. The authors declare no conflicts of interest.

REFERENCES

1. T. B. Pittman, Y. Shih, D. Strekalov, and A. V. Sergienko, *Phys. Rev. A* **52**, R3429 (1995).
2. R. S. Bennink, S. J. Bentley, and R. W. Boyd, *Phys. review letters* **89**, 113601 (2002).
3. J. Cheng and S. Han, *Phys. review letters* **92**, 093903 (2004).
4. A. Gatti, E. Brambilla, M. Bache, and L. A. Lugiato, *Phys. review letters* **93**, 093602 (2004).
5. F. Ferri, D. Magatti, A. Gatti, M. Bache, E. Brambilla, and L. A. Lugiato, *Phys. review letters* **94**, 183602 (2005).
6. Y. Cai and S.-Y. Zhu, *Phys. Rev. E* **71**, 056607 (2005).
7. C. Gao, X. Wang, L. Gou, Y. Feng, H. Cai, Z. Wang, and Z. Yao, *Laser Phys. Lett.* **16**, 065202 (2019).
8. C. Gao, X. Wang, Z. Wang, Z. Li, G. Du, F. Chang, and Z. Yao, *Phys. Rev. A* **96**, 023838 (2017).
9. D.-Z. Cao, J. Xiong, and K. Wang, *Phys. Rev. A* **71**, 013801 (2005).
10. A. Valencia, G. Scarcelli, M. D'Angelo, and Y. Shih, *Phys. review letters* **94**, 063601 (2005).
11. D. Zhang, Y.-H. Zhai, L.-A. Wu, and X.-H. Chen, *Opt. letters* **30**, 2354 (2005).
12. P. B. Dixon, G. A. Howland, K. W. C. Chan, C. O'Sullivan-Hale, B. Rodenburg, N. D. Hardy, J. H. Shapiro, D. Simon, A. Sergienko, R. Boyd *et al.*, *Phys. Rev. A* **83**, 051803 (2011).
13. R. E. Meyers, K. S. Deacon, and Y. Shih, *Appl. Phys. Lett.* **98**, 111115 (2011).
14. S. J. Bentley and R. W. Boyd, *Opt. Express* **12**, 5735 (2004).
15. R. Meyers, K. S. Deacon, and Y. Shih, *Phys. Rev. A* **77**, 041801 (2008).
16. N. Radwell, K. J. Mitchell, G. M. Gibson, M. P. Edgar, R. Bowman, and M. J. Padgett, *Optica* **1**, 285 (2014).
17. D. Pelliccia, A. Rack, M. Scheel, V. Cantelli, and D. M. Paganin, *Phys. review letters* **117**, 113902 (2016).
18. X.-H. Chen, F.-H. Kong, Q. Fu, S.-Y. Meng, and L.-A. Wu, *Opt. letters* **42**, 5290 (2017).
19. P.-A. Moreau, E. Toninelli, P. A. Morris, R. S. Aspden, T. Gregory, G. Spalding, R. W. Boyd, and M. J. Padgett, *Opt. express* **26**, 7528 (2018).
20. S.-Y. Meng, Y.-H. Sha, Q. Fu, Q.-Q. Bao, W.-W. Shi, G.-D. Li, X.-H. Chen, and L.-A. Wu, *Opt. Lett.* **43**, 4759 (2018).
21. W. Gong and S. Han, *Phys. Lett. A* **376**, 1519 (2012).
22. S. W. Hell and J. Wichmann, *Opt. letters* **19**, 780 (1994).
23. M. Tsang and R. Nair, *Optica* **6**, 400 (2019).
24. F. Ferri, D. Magatti, V. Sala, and A. Gatti, *Appl. Phys. Lett.* **92**, 261109 (2008).
25. P. Zhang, W. Gong, X. Shen, D. Huang, and S. Han, *Opt. letters* **34**, 1222 (2009).
26. J. Du, W. Gong, and S. Han, *Opt. letters* **37**, 1067 (2012).
27. Y. Shechtman, S. Gazit, A. Szameit, Y. C. Eldar, and M. Segev, *Opt. letters* **35**, 1148 (2010).
28. J. Chen, W. Gong, and S. Han, *Phys. Lett. A* **377**, 1844 (2013).
29. J. Sprigg, T. Peng, and Y. Shih, *Sci. reports* **6**, 38077 (2016).
30. K. Kuplicki and K. W. C. Chan, *Opt. express* **24**, 26766 (2016).
31. Y. Wang, Y. Zhou, S. Wang, F. Wang, R. Liu, H. Gao, P. Zhang, and F. Li, *Chin. Phys. B* **28**, 044202 (2019).
32. Z. Tong, Z. Liu, C. Hu, J. Wang, and S. Han, *Photonics Res.* **9**, 1069 (2021).
33. F. Wang, C. Wang, M. Chen, W. Gong, Y. Zhang, S. Han, and G. Situ, *Light. Sci. & Appl.* **11**, 1 (2022).
34. H. Ye, Y. Kang, J. Wang, L. Zhang, H. Sun, and D. Zhang, *J. Korean Phys. Soc.* **80**, 964 (2022).
35. Y. Xiao, L. Zhou, and W. Chen, *Opt. Lett.* **47**, 3692 (2022).
36. H. Zhao, X. Wang, C. Gao, Z. Yu, S. Wang, L. Gou, and Z. Yao, *Chin. Opt. Lett.* **20**, 112602 (2022).

FULL REFERENCES

1. T. B. Pittman, Y. Shih, D. Strekalov, and A. V. Sergienko, "Optical imaging by means of two-photon quantum entanglement," *Phys. Rev. A* **52**, R3429 (1995).
2. R. S. Bennink, S. J. Bentley, and R. W. Boyd, "Two-photon coincidence imaging with a classical source," *Phys. review letters* **89**, 113601 (2002).
3. J. Cheng and S. Han, "Incoherent coincidence imaging and its applicability in x-ray diffraction," *Phys. review letters* **92**, 093903 (2004).
4. A. Gatti, E. Brambilla, M. Bache, and L. A. Lugiato, "Ghost imaging with thermal light: comparing entanglement and classical correlation," *Phys. review letters* **93**, 093602 (2004).
5. F. Ferri, D. Magatti, A. Gatti, M. Bache, E. Brambilla, and L. A. Lugiato, "High-resolution ghost image and ghost diffraction experiments with thermal light," *Phys. review letters* **94**, 183602 (2005).
6. Y. Cai and S.-Y. Zhu, "Ghost imaging with incoherent and partially coherent light radiation," *Phys. Rev. E* **71**, 056607 (2005).
7. C. Gao, X. Wang, L. Gou, Y. Feng, H. Cai, Z. Wang, and Z. Yao, "Ghost imaging for an occluded object," *Laser Phys. Lett.* **16**, 065202 (2019).
8. C. Gao, X. Wang, Z. Wang, Z. Li, G. Du, F. Chang, and Z. Yao, "Optimization of computational ghost imaging," *Phys. Rev. A* **96**, 023838 (2017).
9. D.-Z. Cao, J. Xiong, and K. Wang, "Geometrical optics in correlated imaging systems," *Phys. Rev. A* **71**, 013801 (2005).
10. A. Valencia, G. Scarcelli, M. D'Angelo, and Y. Shih, "Two-photon imaging with thermal light," *Phys. review letters* **94**, 063601 (2005).
11. D. Zhang, Y.-H. Zhai, L.-A. Wu, and X.-H. Chen, "Correlated two-photon imaging with true thermal light," *Opt. letters* **30**, 2354–2356 (2005).
12. P. B. Dixon, G. A. Howland, K. W. C. Chan, C. O'Sullivan-Hale, B. Rodenburg, N. D. Hardy, J. H. Shapiro, D. Simon, A. Sergienko, R. Boyd *et al.*, "Quantum ghost imaging through turbulence," *Phys. Rev. A* **83**, 051803 (2011).
13. R. E. Meyers, K. S. Deacon, and Y. Shih, "Turbulence-free ghost imaging," *Appl. Phys. Lett.* **98**, 111115 (2011).
14. S. J. Bentley and R. W. Boyd, "Nonlinear optical lithography with ultra-high sub-rayleigh resolution," *Opt. Express* **12**, 5735–5740 (2004).
15. R. Meyers, K. S. Deacon, and Y. Shih, "Ghost-imaging experiment by measuring reflected photons," *Phys. Rev. A* **77**, 041801 (2008).
16. N. Radwell, K. J. Mitchell, G. M. Gibson, M. P. Edgar, R. Bowman, and M. J. Padgett, "Single-pixel infrared and visible microscope," *Optica* **1**, 285–289 (2014).
17. D. Pelliccia, A. Rack, M. Scheel, V. Cantelli, and D. M. Paganin, "Experimental x-ray ghost imaging," *Phys. review letters* **117**, 113902 (2016).
18. X.-H. Chen, F.-H. Kong, Q. Fu, S.-Y. Meng, and L.-A. Wu, "Sub-rayleigh resolution ghost imaging by spatial low-pass filtering," *Opt. letters* **42**, 5290–5293 (2017).
19. P.-A. Moreau, E. Toninelli, P. A. Morris, R. S. Aspden, T. Gregory, G. Spalding, R. W. Boyd, and M. J. Padgett, "Resolution limits of quantum ghost imaging," *Opt. express* **26**, 7528–7536 (2018).
20. S.-Y. Meng, Y.-H. Sha, Q. Fu, Q.-Q. Bao, W.-W. Shi, G.-D. Li, X.-H. Chen, and L.-A. Wu, "Super-resolution imaging by anticorrelation of optical intensities," *Opt. Lett.* **43**, 4759–4762 (2018).
21. W. Gong and S. Han, "Experimental investigation of the quality of lensless super-resolution ghost imaging via sparsity constraints," *Phys. Lett. A* **376**, 1519–1522 (2012).
22. S. W. Hell and J. Wichmann, "Breaking the diffraction resolution limit by stimulated emission: stimulated-emission-depletion fluorescence microscopy," *Opt. letters* **19**, 780–782 (1994).
23. M. Tsang and R. Nair, "Resurgence of rayleigh's curse in the presence of partial coherence: comment," *Optica* **6**, 400–401 (2019).
24. F. Ferri, D. Magatti, V. Sala, and A. Gatti, "Longitudinal coherence in thermal ghost imaging," *Appl. Phys. Lett.* **92**, 261109 (2008).
25. P. Zhang, W. Gong, X. Shen, D. Huang, and S. Han, "Improving resolution by the second-order correlation of light fields," *Opt. letters* **34**, 1222–1224 (2009).
26. J. Du, W. Gong, and S. Han, "The influence of sparsity property of images on ghost imaging with thermal light," *Opt. letters* **37**, 1067–1069 (2012).
27. Y. Shechtman, S. Gazit, A. Szameit, Y. C. Eldar, and M. Segev, "Super-resolution and reconstruction of sparse images carried by incoherent light," *Opt. letters* **35**, 1148–1150 (2010).
28. J. Chen, W. Gong, and S. Han, "Sub-rayleigh ghost imaging via sparsity constraints based on a digital micro-mirror device," *Phys. Lett. A* **377**, 1844–1847 (2013).
29. J. Sprigg, T. Peng, and Y. Shih, "Super-resolution imaging using the spatial-frequency filtered intensity fluctuation correlation," *Sci. reports* **6**, 38077 (2016).
30. K. Kuplicki and K. W. C. Chan, "High-order ghost imaging using non-rayleigh speckle sources," *Opt. express* **24**, 26766–26776 (2016).
31. Y. Wang, Y. Zhou, S. Wang, F. Wang, R. Liu, H. Gao, P. Zhang, and F. Li, "Enhancement of spatial resolution of ghost imaging via localizing and thresholding," *Chin. Phys. B* **28**, 044202 (2019).
32. Z. Tong, Z. Liu, C. Hu, J. Wang, and S. Han, "Preconditioned deconvolution method for high-resolution ghost imaging," *Photonics Res.* **9**, 1069–1077 (2021).
33. F. Wang, C. Wang, M. Chen, W. Gong, Y. Zhang, S. Han, and G. Situ, "Far-field super-resolution ghost imaging with a deep neural network constraint," *Light. Sci. & Appl.* **11**, 1 (2022).
34. H. Ye, Y. Kang, J. Wang, L. Zhang, H. Sun, and D. Zhang, "High resolution reconstruction method of ghost imaging via surf-nsml," *J. Korean Phys. Soc.* **80**, 964–971 (2022).
35. Y. Xiao, L. Zhou, and W. Chen, "High-resolution ghost imaging through complex scattering media via a temporal correction," *Opt. Lett.* **47**, 3692–3695 (2022).
36. H. Zhao, X. Wang, C. Gao, Z. Yu, S. Wang, L. Gou, and Z. Yao, "Second-order cumulants ghost imaging," *Chin. Opt. Lett.* **20**, 112602 (2022).